Published in final edited form as:
Exp Eye Res. 2010 September ; 91(3): 415–424. doi:10.1016/j.exer.2010.06.018.

Differential susceptibility to experimental glaucoma among 3 mouse strains using bead and viscoelastic injection

Frances E. Cone, **Scott E. Gelman**, **Janice L. Son**, **Mary E. Pease**, and **Harry A. Quigley**
Glaucoma Research Laboratory, Wilmer Institute, Johns Hopkins University School of Medicine, Baltimore, MD USA

Abstract

The purpose of this experiment was to test the susceptibility to retinal ganglion cell (RGC) axon loss and RGC layer cell loss from experimental glaucoma among 3 mouse strains, and between younger and older mice. We obstructed the mouse aqueous outflow channels by injecting 2 μL of 6 μm diameter, polystyrene beads followed by 3 μL of viscoelastic solution into the anterior chamber with a glass micropipette. We evaluated intraocular pressure (IOP) and damage to RGC as measured by optic nerve axon counts and RGC layer neuron counts in 3 strains of young mice (2 month old C57BL/6, DBA/2J, and CD1) and 10 month C57BL/6 mice. Bead and viscoelastic injection produced IOP elevation at ≥1 time point in 94.1% of eyes (112/119), with mean IOP difference from fellow eyes of 4.4 ± 3.0 mmHg. By 6–12 weeks, injected eyes were 10.8% longer and 7.6% wider ($p < 0.0001$). Young DBA/2J and C57BL/6 eyes increased axial length significantly more than young CD1 or older C57BL/6 (all $p \leq 0.02$). RGC layer and axon loss was greatest in CD1 mice, significantly more than the other groups (p from 0.04 to <0.0001). Young C57BL/6 eyes elongated more and lost more RGC layer cells than older C57BL/6 mice ($p = 0.02$ and 0.01, respectively). With this mouse glaucoma model, there was differential susceptibility to ocular elongation and RGC layer and axon damage among mouse strains and by age. Factors that determine sensitivity to RGC injury can be studied using transgenic mouse strains with inducible models.

Keywords

glaucoma; mouse; experimental; retina; ganglion cells; polystyrene beads; aqueous outflow channels

Introduction

Glaucoma is the second leading cause of vision loss worldwide (Quigley and Broman, 2006). To understand its pathogenesis and to improve glaucoma therapy, animal models of glaucoma were developed in monkeys (Gaasterland and Kupfer, 1974; Quigley and Addicks, 1980; Quigley and Hohman, 1983) and rats (Shareef et al., 1995; Morrison et al., 1997; Sawada and Neufeld, 1999; Mittag et al., 2000; Schori et al., 2001; Ueda et al., 1998; Moreno et al., 2004) often using laser treatment to the trabecular meshwork to increase intraocular pressure (IOP). Similar laser treatment to the mouse anterior segment has been used to increase IOP (Grozdanic et al., 2003; Aihara et al., 2003b; Gross et al., 2003; Nakazawa et al., 2006), as

Correspondence: Dr. Harry A. Quigley, Wilmer 122, 600 North Wolfe Street, Johns Hopkins Hospital, Baltimore, MD 21287; hquigley@jhmi.edu; Phone: (410) 955-2777; Fax: (410) 955-2542.

have occlusion of episcleral veins (Ruiz-Ederra and Verkman, 2006) and injection of hypertonic saline into episcleral vessels (McKinnon et al., 2009). Improvements in the reliability of induced damage and in the minimization of collateral ocular damage would facilitate glaucoma research. Spontaneous glaucoma occurs in the certain mammals, including beagle dogs (Samuelson et al., 1989) and 3 mouse strains (John et al., 1998; Aihara et al., 2003a; Zhou et al., 2008). However, inducible mouse glaucoma models permit study of the effect of experimental disease in existing and transgenic strains without time-consuming cross-breeding.

The optimal mouse glaucoma model would have the following features: 1) prompt, consistent increased IOP in most eyes; 2) lack of detrimental effects on the cornea and sclera; 3) death of RGC, but not of other retinal neurons; and 4) ease and low cost of implementation. Previous investigators have obstructed the outflow channels by injecting either latex spheres in monkeys (Weber et al., 2001), polystyrene beads in rats and mice (Sappington et al., 2010), and repeated injections of latex microspheres with hydroxypropylmethylcellulose into rats (Urcola et al., 2006). We modified this approach by a single injection of polystyrene beads followed immediately by a viscoelastic substance in mouse eyes, a model that satisfies the above criteria. The development of a non-invasive tonometer to measure IOP accurately in mice was an important facilitating step (Goldblum et al., 2002; Pease et al., 2006). Its accuracy in glaucomatous mice was confirmed in a companion report (M.E. Pease, personal communication, 2010).

Susceptibility to glaucoma injury in humans is related to several known risk factors, including older age, ethnicity, central corneal thickness, and axial length (Boland and Quigley, 2007). We tested the effect of our mouse glaucoma model on both younger and older mice of one pigmented strain (C57BL/6) and compared the results to that of young mice of two other strains, the pigmented DBA/2J and the albino CD1. Our purpose was to determine the generalizability of the glaucoma model, as well as to compare cell loss in the retinal ganglion cell (RGC) layer and optic nerve across strains to identify differences in susceptibility.

Methods

Animals

A total of 168 female mice were utilized in this study. Ninety-seven were 8 week old C57BL/6, 25 were 8 month old C57BL/6, 25 were 8 week old DBA/2J, and 21 were 8 week old CD1. Two mice died due to anesthesia complications and 9 were euthanized due to severe ocular enlargement with corneal exposure or ulceration, leaving a total of 157 mice that provided data. All animals were treated in accordance with the ARVO Statement for the Use of Animals in Ophthalmic and Vision Research, using protocols approved and monitored by the Johns Hopkins University School of Medicine Animal Care and Use Committee.

Methods tested for bead injection

Sappington et al. (2010) reported injection of beads into the anterior chamber with successful production of chronically elevated IOP in mice. We noted that in our hands a variable number of the beads exited the anterior chamber when we removed the glass cannula with bead injection in aqueous solution. On the assumption that retention of injected beads would be desirable, we added an injection of viscoelastic substance to push the beads into the anterior chamber angle. We also tested several variables to optimize the protocol, using Polybead Microspheres® (Polysciences, Inc., Warrington, PA, USA) of 1, 3 and 6 μm diameter and testing the effects of pupil dilation, ocular exposure during surgery, cannula size (50 or 100μm tip width), age and strain of mice, bead concentration and volume, and the use of a viscoelastic solution

following bead injection (10 mg/ml sodium hyaluronate: Healon, Advanced Medical Optics Inc., Santa Ana, CA, USA).

In the optimal procedure, which had the most consistent IOP elevation and least adverse effects, we first sterilized the beads, by placing them in 100% ethanol in 0.5mL Epindorf tubes. They were centrifuged, resuspended in alcohol, and recentrifuged and resuspended twice in sterile, phosphate buffered saline (PBS). The final pellet was aspirated as a confluent solution from the pellet directly into a glass micropipette used for injection (3×10^6 beads per μL for 6 μm beads). Mice were anesthetized with intraperitoneal injection of ketamine, xylazine, and acepromazine (50, 10 and 2 mg/kg, respectively). A 50μm glass cannula, connected by tubing to a Hamilton syringe (Hamilton Company Reno, NV, USA), was first filled with 3 μL of viscoelastic solution, then 0.05 μL of air, and finally 2μL of 6μm beads. This allowed the beads to be injected first, followed by the viscoelastic. The air prevented mixture of beads with viscoelastic, though this admixture is minimal even without the air, since the cannula/tubing/needles were prepared just before injection. The left eye was proptosed and the glass cannula was inserted into the inferior portion of the left anterior chamber. The fluid was slowly injected over 45 seconds, and the empty cannula was left in place for two minutes to minimize efflux of injected material.

IOP measurements were made in both eyes with the TonoLab tonometer (TioLat, Helsinki, Finland) under combined topical anesthesia with 0.5% proparacaine hydrochloride eyedrops (Akorn Inc, Buffalo Grove, IL, USA) and general anesthesia (as above). IOP was measured prior to bead injection (baseline), 10–30 minutes after injection (in selected animals), and in all animals 3 days after injection and weekly thereafter until 6 or 12 weeks after injection.

Sacrifice and Axial Length Measurements

Animals were sacrificed under general anesthesia by exsanguination and intracardiac perfusion of 4% paraformaldehyde in 0.1M sodium phosphate buffer (Na_3PO_4, pH =7.2). Enucleated eyes were inflated to 15mmHg with a needle connected to a fluid-filled reservoir for measurement of axial length and width with a digital caliper (Instant Read Out Digital Caliper, Electron Microscopy Sciences, Hatfield, PA, USA). The length was measured from the center of the cornea to a position just temporal to the optic nerve, while width was measured at the largest dimension at the equator, midway between cornea and optic nerve.

Optic Nerve Axon Counts

One primary outcome measure to assess RGC damage was axon loss. After perfusion fixation, globes and optic nerves were placed in 1% osmium, dehydrated in ascending alcohol concentration, and placed in 1% uranyl acetate in 100% ethanol for 1 hour. Tissues were embedded in epoxy resin mixture at 60°C for 48 hours. One micron thick cross-sections of the optic nerve and retinal/optic nerve segments were stained with 1% toluidine blue in 1% sodium borate. Digital images of the nerves were taken at low power to measure the total optic nerve area in each nerve and then at 100× using a Cool Snap camera and Metamorph Image Analysis software. For each nerve, five 40 × 40 μm fields were acquired, equaling a 9% sample of the total nerve area. Masked observers edited non-axonal elements from each image, generating an axon density measure from the software. Average axon density/mm^2 was multiplied by the individual nerve area to estimate axon number. Nerve area and density were calculated for each nerve. Experimental eyes were compared to the mean axon number in pooled, fellow eye nerves of the appropriate strain, length of glaucoma, and tissue fixation to yield percent axon loss.

RGC Layer Counts

To corroborate the axon count data, we also counted RGC layer cells in flat mounts of both glaucoma and fellow control eyes. Both retinas were removed from perfusion-fixed eyes,

incised for flat mounting, placed on SuperFrost Plus slides for 24 hours, washed in PBS for 10 minutes, and treated with 0.1% Triton/PBS for 5 minutes before being exposed to 1:250 dilution of DAPI stain for 5 minutes (Invitrogen, Carlsbad, CA, USA). After buffer washes, retinas were cover-slipped with Fluorescent Mounting Medium (DakoCytomation, Carpinteria, CA, USA) and imaged using the Zeiss LSM 510 Meta Confocal Microscope (Zeiss MicroImaging, Thornwood, NY, USA). Twelve 40× images were taken per retina, 3 fields from each of 4 quadrants (superior, nasal, inferior, temporal), equaling a 4% sample of total retinal area. Each image was taken at the level of the RGC layer and analyzed with Metamorph Image Analysis software (Molecular Devices, Downington, PA, USA). Because the confocal imaging was performed only at the level of the RGC layer, astrocytes of the nerve fiber layer are not included. All cells with a round or slightly oval nucleus and morphology compatible with that of neurons were identified manually by trained technical staff masked to the protocol details for each retina. Interobserver reproducibility of the method comparing 3 technicians showed a mean difference of only 0.5% between observer A and B, and a mean difference of 1.7% between observer A and observer C, counting a total of nearly 6,000 cells from 12 images in each test. Cells that were not counted included: 1) those with elongated nuclei more typical for endothelial cells or astrocytes and 2) polymorphonuclear cells assumed to be white blood cells. Experimental retinas were compared to mean RGC layer counts from pooled, fellow eyes matched for strain, length of glaucoma, and fixation protocol.

Histology

We quantitatively measured mid-retinal and outer retinal layer thickness to evaluate possible damage other than to the RGC layer and nerve fiber layer—features that might indicate retinal vascular compromise that would be undesirable in a glaucoma model. Samples of the optic nerve head and adjacent retina from both injected and fellow control eyes were epoxy embedded with same protocol as for optic nerve cross-sections above. The thickness of the inner nuclear and outer nuclear layers of the retina were measured at 6 locations on each section by a masked observer in 15 mice (5 from each of the 3 strains) in paired injected and control eyes.

Selected eyes underwent sectioning to determine the position of beads 6 and 12 weeks after injection in epoxy embedded tissues.

Statistical Methods

The following data were tabulated and compared between treated and control eyes in each animal: axial length and width, IOP average level, IOP exposure over time (positive integral = area under the IOP over time curve in the treated eye that exceeded the area under the IOP curve in the control eye), number of weekly measures exceeding the 97.5% confidence limit for normal intraocular difference (5 mm Hg), RGC layer cell count, and axon count. Primary outcomes were compared taking into account height and length of IOP exposure (6 or 12 weeks), age, and strain. Mean values were compared with parametric statistical tests for data that were normally distributed and median values with non-parametric testing for those whose distributions failed normality testing.

Results

IOP Data

Prior to determining the optimal protocol, we used 57 young C57BL/6 mice in trials of various permutations of the methods. IOP data for 9 of these preliminary animals, which were sacrificed 3 weeks after bead injection, are shown with the 4 groups of mice in which the optimal injection protocol was used (young and older C57BL/6, young DBA/2J, and young CD1; Table 1).

In normal, paired mouse eyes under anesthesia, the 97.5% confidence interval for IOP difference between eyes was ≥ 5 mm Hg. We used this level as one of several benchmarks for measuring the IOP elevation produced by the model. Overall, injected eyes exceeded this criterion difference 42% of the time, with group data for this statistic varying from 21—70% (percent IOP elevations, Table 1). The final bead injection procedure effectively produced IOP elevation on one or more of the 7 measurements in the 6 week group or 13 measurements in the 12 week group in 94% (112/119) of animals. The mean difference between injected and control eyes at 6 and 12 weeks after injection were generally 50% or more above the normal IOP level of ~10–11 mmHg, as measured under anesthesia (Table 1). To assure that IOP was not dramatically elevated immediately after bead injection, in one group of 6 animals we measured IOP during the first 30 minutes after bead injection. Values ranged from 6–12 mmHg. The elevations in IOP were only occasionally over 30 mmHg during the 6–12 week experiments.

The time course for mean IOP elevation was steady, as shown for C57BL/6 older mice (Figure 1). Graphs for the other 3 groups of mice, as seen in Figure 1, were similar in configuration. The positive integral IOP value was calculated as the difference between the bead-injected eye and its fellow eye, integrating the sum of the area under a curve that expressed the difference in IOP between the eyes in units of mm Hg—days, but including only those times when IOP was higher in the bead-treated eye. The positive integral for animals at 6 weeks was 146 ± 57 mm Hg--days (61 mice) and at 12 weeks = 325 ± 98 mm Hg—days, showing a significant cumulative increase in IOP exposure over time ($p < 0.0001$, t test; Table 1). The positive integral compared among the strains was not significantly different at either 6 or 12 weeks (analysis of variance, $p = 0.08$ and $p = 0.15$, respectively). In analyses of RGC layer loss and axon loss, we included the IOP exposure over time as an individual value for each animal in the multivariable linear regression analyses.

Histology

Using light microscopy, we found that many beads remained in the anterior chamber for 3 months, as was obvious clinically (Figure 2B). Beads were also found in the aqueous outflow channels of the limbus and in the suprachoroidal space, suggesting that the mechanism for IOP elevation was obstruction of both the trabecular and uveoscleral outflow pathways. In most eyes examined, there were no visible inflammatory cells.

Examination of sections of the retina in bead-injected eyes showed only loss of cells from the RGC layer and thinning of the nerve fiber layer. As expected in glaucomatous optic neuropathy, there was no thinning in the inner nuclear or outer nuclear or photoreceptor layers (Figure 3B). The mean thickness of the outer nuclear layer in bead-injected compared to fellow, control eyes differed by only 2.8% (larger), while the inner nuclear layer differed by −1.4% (smaller), and both were statistically insignificant differences ($p = 0.37$ and 0.9, t test).

Axial Length Data

In bead-injected eyes, axial length and width measured post-mortem significantly increased, from 4 to 25% in each mouse strain (Table 2, 3). The increase was greatest in DBA/2J mice, followed by C57BL/6 young mice. It was similar in magnitude in C57BL/6 older and CD1 young animals. The increase was statistically significant compared to fellow, control eyes in every strain except the CD1, 12 week group ($p = 0.08$). Mean width also enlarged significantly, but significantly less than length ($p = 0.003$, paired t test, $n = 76$).

To compare the enlargement of bead glaucoma model eyes to that in spontaneous glaucoma DBA/2J mice, we measured 57 eyes of 35 DBA/2J animals of mean age = 55.7 ± 7.0 weeks that had spontaneous glaucoma and no bead injections, measured identically post-mortem, and

compared them to young, control DBA/2J eyes (2–4 months of age, prior to IOP elevation). The estimated mean elongation in the older compared to younger DBA/2J eyes was 14.3%, very similar to that of DBA/2J young eyes that underwent bead model glaucoma (overall average for 6 and 12 week eyes = 16.7% (Table 3), difference between older DBA/2J and bead-injected DBA/2J, $p > 0.05$).

When axial length data were compared across strains, DBA/2J had significantly greater elongation than younger and older C57BL/6 and CD1, while C57BL/6 young mice had more elongation than C57BL/6 older and CD1 mice (Table 3). It is unlikely that the differences in elongation might derived from different IOP exposure among strains, as there were no statistically significant differences in that variable across strains (see above). Nonetheless, we carried out multivariable linear regression analysis of axial elongation, controlling for the exposure to IOP (positive integral IOP) in each eye and by strain. The increase in globe size remained significantly greater in DBA/2J eyes than in either older C57BL/6 or in CD1 animals in these regression models (Table 3). The difference between C57BL/6 younger mice and either C57BL/6 older or CD1 mice remained close to statistically significant. The relationship of axial length increase to positive integral IOP for all model glaucoma eyes indicated that this relationship explained only a small portion of the variability in axial elongation (linear regression $r^2 = 0.08$).

Enlargement of the cornea and globe was often clinically evident 3 days after bead injection, and corneal neovascularization and limbal staphyloma development were common. In 7.6% (9/119) of mice, cornea thinning and/or ulceration were severe enough to necessitate sacrifice prior to the planned intervals of 6 or 12 weeks.

Axon Loss

Axon count data showed that loss of RGC axons was significant in most strains, even when only the individual groups of 10–14 animals at a particular time point were considered (Table 4). The older C57BL/6 strain was exceptional in having no significant axon loss. Furthermore, the greatest median loss at 6 and 12 weeks was in CD1 mice, followed by C57BL/6, DBA/2J, and least in C57BL/6 older mice (Table 4). This ranking of percent axon loss by strain remained the same when multivariable models were constructed to take IOP exposure into account (Table 5). In these models, axon loss compared to control was statistically significant in 3 mouse groups (CD1, young C57BL/6, and DBA/2J), but not in C57BL/6 older mice (Table 5). The values for axon loss showed a significant effect of mouse strain (one-way ANOVA, $p= 0.02$; Table 5), with greater loss among the CD1 animals than the DBA/2J and C57BL/6 older mice. When axon loss was compared with adjustment for IOP exposure, the greater loss among CD1 mice was less significant overall, though still different from C57BL/6 older mice.

The loss of axons in damaged nerves was clearly seen in epoxy-embedded cross-sections as a reduction in the normal dark rings of myelin surrounding clear axoplasm, and the appearance of degenerating axons and macrophages filled with clear vacuoles (Figure 4).

RGC layer cell loss

The loss of neurons from the RGC layer confirmed the axon count data in both magnitude and the pattern of susceptibility of the mouse strains. Mean RGC layer loss varied from 9.9% (CD1) to no loss (C57BL/6 old) in the 6 week groups, and from 20.1% to 4.1% at 12 weeks (Table 4). Likewise, the median loss of RGC layer cells in both 6 and 12 week time periods was greatest in CD1 and declined in the order C57BL/6 young, DBA/2J young, C57BL/6 older, just as did the axon loss data.

To take account of differences in IOP exposure and length of experiment in comparing across strains, we constructed linear regression models with RGC layer cell loss as dependent variable and positive integral IOP as independent variable. RGC layer loss was significant compared to fellow, control eyes in 3 of the 4 strains of mice: CD1, young C57BL/6, and DBA/2J, but not older C57BL/6 (Table 6). The loss differed significantly among strains of mice (Kruskal-Wallis test, $p = 0.001$). Just as in the axon loss data, the CD1 animals had the greatest loss and older C57BL/6 had the least. In pair-wise comparisons, the mean loss in CD1 mice was significantly greater than that in the other 3 strains, and the difference between younger and older C57BL/6 mice was significant (Table 6). These intergroup differences remained significant when comparisons were adjusted for IOP exposure (Table 6). RGC layer loss and axon loss were significantly related by linear regression ($p < 0.0001$, $r = 0.43$), again confirming that the two measures lead to similar conclusions as to the amount of damage and the susceptibility by strain and age.

The exposure of each mouse strain to IOP over time was not well correlated with RGC layer cell loss (all r^2 less than 0.2). Likewise, there was modest correlation between RGC layer cell loss and axial elongation (Spearman $r = 0.20$, $p = 0.08$, $n = 80$ eyes).

Three retinas (one from each strain) had more DAPI-labeled RGC layer nuclei than the mean in control, fellow eyes. Careful inspection showed that this was due to the presence of polymorphonuclear leukocytes, which extended into the outer retinal layers (Figure 5D). We concluded that these retinas had either inflammation or infection and excluded their data.

Previous investigations have confirmed that the total RGC layer counts correspond well to the optic nerve grading of cell loss in mouse glaucoma (Jakobs et al., 2005). It is well known that many neurons in the RGC layer are amacrine cells and are included in our counts of DAPI-stained neurons. We chose not to backfill RGC with dye from the superior colliculus, since doing so at the beginning of a 12 week period leads to non-specific dye uptake by non-neurons that phagocytose dead, fluorescent RGCs. These non-RGC must be manually identified to avoid inclusion as RGC (Blair et al., 2005). Backfilling later, during high IOP, leads to inconsistent filling and underestimation of remaining RGC (Salinas-Navarro et al., 2010). The specific RGC markers for normal RGC (Thy-1, brn3, and synuclein gamma (Sncg)) are rapidly down-regulated with injury, leading to possible underestimation of RGC numbers (Yang et al., 2007). The number of amacrine cells is unaffected by RGC loss in experimental rat glaucoma (Kielczewski et al., 2005). In addition, Jakobs et al. (2005) concluded that total neuron counts from the RGC layer by DAPI staining combined with specific labeling of other retinal neurons revealed no cell loss (including amacrine cells) other than RGC in the DBA/2J mouse. This suggests that most dying RGC layer cells in mouse glaucoma models would be RGC. Thus, the estimated loss of RGC would be derivable from the proportions of RGC layer cells that are amacrines and RGC in the mouse, estimated to be 59% amacrines and 41% RGC (Jeon et al., 1998). To confirm that the proportion of RGC layer cells that are RGC in the mouse strains utilized, we carried out *in situ* hybridization for Sncg (a known RGC marker) in normal C57BL/6 retinas (protocol used from Soto et al., 2008). Thirty-two percent of RGC layer cells labeled with this RGC marker. Counts in retinas from 12 month DBA/2J mice with prolonged, spontaneous glaucoma damage found only 2.3% and 0.7% of RGC layer cells labeled for Sncg, and the number of remaining neurons (negative for Sncg) was 59% of the number in normal whole mounts, as would be expected from the data of Jeon et al. (1998). Taken together, these data suggest that 40% of RGC layer cells in the mouse strains studied are RGC. When we calculated the ratio of RGC layer cell loss to axon count loss in 75 mice with both retinal and optic nerve data for the same eye, the median ratio of RGC layer to axon loss was 0.34 (as would be expected if ~40% of RGC layer cells were RGC as estimated by Sncg labeling).

Discussion

The 3 different strains of mice and 2 age groups of the C57BL/6 strain showed significant differences in response to chronic IOP elevation that may provide important clues in glaucoma pathogenesis. First, the axial length and width of the mouse eye rapidly increased with chronic IOP elevation, as do the eyes of human infants, and to a lesser degree monkey and rat eyes with experimental glaucoma. This fixed deformation began within the first week and was not reversed in those eyes that returned to normal IOP. The eyes of young DBA/2J and young C57BL/6 mice elongated significantly more than those of young CD1 mice or older C57BL/6 mice, and this trend remained when IOP exposure was taken into account. In fact, the elongation in DBA/2J mice with bead-injection glaucoma was similar in magnitude to that observed when spontaneous glaucoma is allowed to occur in older DBA/2J mice over 12 months.

The resistance to elongation in older C57BL/6 animals seems consistent with increased stiffness in connective tissues with age. Indeed, we have measured increased stiffness in older compared to younger C57BL/6 mice in acute biomechanical inflation testing (K. Myers, Ph.D.: personal communication, 2009). However, there may be a complex relationship between the baseline biomechanical behavior of the tissues in young and old animals, on the one hand, and the degree of elongation of the globe with chronic IOP elevation. Both short-term responsiveness and permanent elongation may participate in RGC and axon injury, separately and in combination. For example, axial elongation after weeks of IOP elevation would be a result not only of immediate tissue response, but also damage and repair processes in the ocular connective tissues that might be age-related or strain specific. Deformation of the ocular wall might produce damage to RGC axons as they pass through the optic nerve head. The larger the globe at any IOP, the greater the mechanical strain induced in the sclera to be transmitted to the nerve head. Alternatively, the eye might be made safer from chronic IOP elevation by globe enlargement, if the scleral expansion somehow lessened injury to RGC and their axons.

Comparing our RGC and axon loss data to the mean axial elongation in each group does not give consistent support for either of these two alternative hypotheses. The axial elongation was least in CD1 and older C57BL/6 animals. Yet, CD1 had the most RGC and axon loss and older C57BL/6 had the least. From this, one might conclude that factors other than scleral elongation explain the dramatically greater susceptibility to neuronal damage from experimental glaucoma in the CD1 animals. On the other hand, among C57BL/6 mice, the young animals had more axial elongation as well as greater RGC layer cell loss compared to older animals of the same strain. This suggests that, in this mouse strain, failure to undergo progressive ocular elongation was associated with a protective effect. There may be important strain differences in how axons and RGC bodies upregulate their survival and death mechanisms.

We refer here to 2–4 month old and 10–12 month old mice as “younger” and “older”, though laboratory mice can live 2 years or more. It would be incorrect to assume that the older mice used were directly comparable to elderly humans, who have a higher prevalence of glaucoma than young persons. Clearly, many factors, including IOP level, lead older humans to be more susceptible to incident glaucoma than those who are younger. This does not necessarily mean that artificially increased IOP alone (as in animal models) would produce greater RGC loss in older compared to younger persons. The comparable question in humans would be to ask whether a child at age 10 is more susceptible to RGC injury at a chronic IOP of 35 mm Hg than is a 70 year old. To our knowledge, this has never been shown and would be difficult to ascertain. We hope to study age-related differences in glaucoma susceptibility in mice to gain clues as to which features may be worth investigating as risk factors in humans.

We found that both axon loss and RGC layer loss occurred in mice with this model, that the two outcomes were significantly correlated in 75 eyes in which both were measured, and that the relative susceptibility among the 4 groups of mice (3 strains and 2 ages of C57BL/6) was identical with both measurements. This strongly points to the validity of the concept that variations in susceptibility to increased IOP can be studied with this model. Since RGC body loss and RGC axon loss may differ in mechanism and temporally, axon loss occurring first in some models (Libby et al., 2005), we plan further study of the two processes, with more specific identification of RGC type and behavior. When we compared the relative loss of RGC layer cells and axons, estimating the effect of amacrines included in DAPI counts, the loss of RGC bodies was somewhat greater than axon loss. While the retinal whole mount technique permits rapid evaluation, our additional studies of the sequence of death between cell body and axon will include of more time points and more specific labeling for RGC.

We used positive integral IOP as an estimate of exposure, but found that it was not tightly correlated with RGC or axon loss. This could mean that weekly sampling of IOP was inadequate to characterize IOP exposure differences. A lack of correlation between measured IOP and RGC loss was also noted in DBA/2J spontaneous glaucoma mice by Scholz et al. (2008), though Inman et al. (2006) found a good correlation in the same model using TonoPen IOP measurement. The IOP injury to RGC in mice may derive from unmeasured IOP elevations. An alternative hypothesis is that the TonoLab did not accurately reflect true IOP in the glaucomatous mouse eye. We had previously corroborated its accuracy in normal mice (Goldblum et al., 2002). We, therefore, conducted a detailed calibration study of the TonoLab in all three strains: young CD1, and both young and older C57BL/6, and young and old DBA/2J. The data, presented in a companion report (M.E. Pease, personal communication, 2010), show that IOP is accurately represented by the TonoLab in bead-induced glaucoma eyes and in spontaneous DBA/2J glaucoma eyes.

Ideal attributes for a mouse glaucoma model would include efficient production of IOP elevation and typical damage to RGC without causing undesirable side effects. Spontaneous glaucoma in the DBA/2J mouse has been a useful model, but to study the importance of other genetic influences using knockout or gene-modified strains, cross-breeding with DBA/2J is needed. The spontaneous glaucoma, collagen 1 deficient mice were recently re-derived to improve breeding efficiency (Dai et al., 2009). Our bead and viscoelastic method is a modification of that reported by Sappington et al. (2010), designed to avoid a problem we had with bead reflux when the injection cannula was removed. This modified model induced chronic IOP elevation with a minimum of collateral damage to the mouse eye. Many animals had sufficient IOP elevation to induce loss of RGC axons and loss of neurons and this occurred only in the RGC layer, as in human glaucoma. Our method can be readily learned by technical staff.

There are weaknesses of the bead injection model that may be amenable to future improvement, though to some degree this may be limited by the features of the mouse eye. First, IOP elevation is modest in most eyes (under anesthesia), and when severe IOP elevation does occur, the cornea can ulcerate and require sacrifice of the animal, as in 7% of our mice. There are fluctuations in IOP in bead-injected eyes and this variability is relatively undesirable. However, in our experience with animal glaucoma models, variability among animals and within the same eye over time is common and to some degree unavoidable, since the method disturbs the normal equilibrium of aqueous flow. Since the beads fill the anterior chamber, imaging of the retina and optic nerve head *in vivo* is difficult. However, we found that corneal opacity and poor pupil dilation can occur after laser-induced and spontaneous glaucoma in the mouse, so this may be a general problem. The measurements of axial length and width were performed on eyes that had just been fixed with aldehyde, in order to preserve retinal and optic nerve structure—our primary outcome. Fixation could have altered the dimensions achieved by

inflation to 15 mm Hg compared to unfixed tissue. Since both control and injected eyes were fixed identically, this would be a serious problem only if there were differential shrinkage in glaucoma compared to normal eyes. We are now engaged in separate studies of biomechanical behavior in glaucoma mice that will compare the present length/width data to that in unfixed eyes.

In summary, bead and viscoelastic injection in mouse eyes produced a useful model of experimental glaucoma. Differences among mouse strains and with age were significant, suggesting that the method could be productively used to measure differences in structural or biochemical risk factors between genetically altered or pharmacologically treated mouse strains over experimental periods as short as 6 weeks with modest numbers of animals.

Acknowledgments

Supported in part by Public Health Service Research Grants EY02120 and EY 01765 (Dr Quigley and Wilmer Institute), the Leonard Wagner Charitable Trust, William T. Forrester, and Alcon Laboratories, Ft. Worth TX.

Don Zack, MD PhD provided advice and manuscript review. David Calkins, PhD and Martin Wax, MD PhD provided important ideas that initiated this investigation.

References

Aihara M, Lindsey JD, Weinreb RN. Ocular hypertension in mice with a targeted type 1 collagen mutation. Invest Ophthalmol Vis Sci 2003a;44:1581–1585. [PubMed: 12657595]

Aihara M, Lindsey JD, Weinreb RN. Experimental mouse ocular hypertension: establishment of the model. Invest Ophthalmol Vis Sci 2003b;44:4314–4320. [PubMed: 14507875]

Blair M, Pease ME, Hammond J, Valenta D, Kielczewski J, Levkovitch-Verbin H, Quigley HA. Effect of glatiramer acetate on primary and secondary degeneration of retinal ganglion cells in the rat. Invest Ophthalmol Vis Sci 2005;46:884–890. [PubMed: 15728544]

Boland MV, Quigley HA. Risk factors and open-angle glaucoma: concepts and applications. J Glaucoma 2007;16:406–418. [PubMed: 17571004]

Dai Y, Lindsey JD, Duong-Polk X, Nguyen D, Hofer A, Weinreb RN. Outflow facility in mice with a targeted type I collagen mutation. Invest Ophthalmol Vis Sci 2009;50:5749–5753. [PubMed: 19797236]

Gaasterland D, Kupfer C. Experimental glaucoma in the rhesus monkey. Invest Ophthalmol 1974;13:455–457. [PubMed: 4208801]

Goldblum D, Kontiola AI, Mittag T, Chen B, Danias J. Non-invasive determination of intraocular pressure in the rat eye. Comparison of an electronic tonometer (TonoPen), and a rebound (impact probe) tonometer. Graefe's Arch Clin Exp Ophthalmol 2002;240:942–946. [PubMed: 12486518]

Gross RL, Ji J, Chang P, Pennesi ME, Yang Z, Zhang J, Wu SM. A mouse model of elevated intraocular pressure: retina and optic nerve findings. Trans Am Ophthalmol Soc 2003;101:163–169. [PubMed: 14971574]

Grozdanic SD, Betts DM, Sakaguchi DS, Allbaugh RA, Kwon YH, Kardon RH. Laser-induced mouse model of chronic ocular hypertension. Invest Ophthalmol Vis Sci 2003;44:4337–4346. [PubMed: 14507878]

Inman DM, Sappington RM, Horner PJ, Calkins DJ. Quantitative correlation of optic nerve pathology with ocular pressure and corneal thickness in the DBA/2 mouse model of glaucoma. Invest Ophthalmol Vis Sci 2006;47:986–996. [PubMed: 16505033]

Jakobs TC, Libby RT, Ben YU, John SWM, Masland RH. Retinal ganglion cell degeneration is topological but not cell type specific in DBA/2J mice. J Cell Biol 2005;171:313–325. [PubMed: 16247030]

Jeon CJ, Strettoi E, Masland RH. The major cell populations of the mouse retina. J Neurosci 1998;18:8936–8946. [PubMed: 9786999]

John SW, Smith RS, Savinova OV, Hawes NL, Chang B, Turnball D, Davisson M, Roderick TH, Heckenlively JR. Essential iris atrophy, pigment dispersion, and glaucoma in DBA/2J mice. Invest Ophthalmol Vis Sci 1998;39:951–962. [PubMed: 9579474]

Kielczewski JL, Pease ME, Quigley HA. The effect of experimental glaucoma and optic nerve transection on amacrine cells in the rat retina. Invest Ophthalmol Vis Sci 2005;46:3188–3196. [PubMed: 16123418]

Levkovitch-Verbin H, Quigley HA, Martin KRG, Valenta D, Kerrigan-Baumrind LA, Pease ME. Translimbal laser photocoagulation to the trabecular meshwork as a model of glaucoma in rats. Invest Ophthalmol Vis Sci 2002;43:402–410. [PubMed: 11818384]

Libby RT, Li Y, Savinova OV, Barter J, Smith RS, Nickells RW, John SW. Susceptibility to neurodegeneration in a glaucoma is modified by Bax gene dosage. PLoS Genet 2005;1:17–26. [PubMed: 16103918]

McKinnon SJ, Schlamp CL, Nickells RW. Mouse models of retinal ganglion cell death and glaucoma. Exp Eye Res 2009;88:816–824. [PubMed: 19105954]

Mittag TW, Danias J, Pohorenec G, Yuan HM, Burakgazi E, Chalmers-Redman R, Podos SW, Tatton WG. Retinal damage after 3 to 4 months of elevated intraocular pressure in a rat glaucoma model. Invest Ophthalmol Vis Sci 2000;41:3451–3459. [PubMed: 11006238]

Moreno MC, Campanelli J, Sande P, Sánez DA, Keller Sarmiento MI, Rosenstein RE. Retinal oxidative stress induced by high intraocular pressure. Free Radic Biol Med 2004;37:803–812. [PubMed: 15384194]

Morrison JC, Moore CG, Deppmeier LM, Gold BG, Meshul CK, Johnson EC. A rat model of chronic pressure-induced optic nerve damage. Exp Eye Res 1997;64:85–96. [PubMed: 9093024]

Nakazawa T, Nakazawa C, Matsubara A, Noda K, Hisatomi T, She H, Michaud N, Hafezi-Moghadam A, Miller JW, Benowitz LI. Tumor necrosis factor-alpha mediates oligodendrocyte death and delayed retinal ganglion cell loss in a mouse model of glaucoma. J Neurosci 2006;26:12633–12641. [PubMed: 17151265]

Pease ME, Hammond J, Quigley HA. Manometric calibration and comparison of TonoLab and TonoPen tonometers in rats with experimental glaucoma and in normal mice. J Glaucoma 2006;15:512–519. [PubMed: 17106364]

Quigley HA, Addicks EM. Chronic experimental glaucoma in primates. II. Effect of extended intraocular pressure on optic nerve head and axonal transport. Invest Ophthalmol Vis Sci 1980;19:137–152. [PubMed: 6153173]

Quigley HA, Hohman RM. Laser energy levels for trabecular meshwork damage in the primate eye. Invest Ophthalmol Vis Sci 1983;24:1305–1306. [PubMed: 6885314]

Quigley HA, Broman A. The number of persons with glaucoma worldwide in 2010 and 2020. Br J Ophthalmol 2006;90:151–156.

Ruiz-Ederra J, Verkman AS. Mouse model of sustained elevation in intraocular pressure produced by episcleral vein occlusion. Exp Eye Res 2006;82:879–884. [PubMed: 16310189]

Salinas-Navarro M, Alarcón-Martínez L, Valente-Sonano FJ, Jiménez-López M, Mayor- Torroglosa S, Avilés-Trigueros M, Villegas-Pérez MP, Vidal-Sanz M. Ocular hypertension impairs optic nerve axonal transport leading to progressive retinal ganglion cell degeneration. Exp Eye Res 2010;90:168–183. [PubMed: 19835874]

Samuelson DA, Gum GG, Gelatt KN. Ultrastructural changes in the aqueous outflow apparatus of beagles with inherited glaucoma. Invest Ophthalmol Vis Sci 1989;30:550–561. [PubMed: 2925324]

Sappington RM, Carlson BJ, Crish SD, Calkins D. The microbead occlusion model: A paradigm for induced ocular hypertension in rats and mice. Invest Ophthalmol Vis Sci 2010;51:207–216. [PubMed: 19850836]

Sawada A, Neufeld AH. Confirmation of the rat model of chronic, moderately elevated intraocular pressure. Exp Eye Res 1999;69:525–531. [PubMed: 10548472]

Scholz M, Buder T, Seeber S, Adamek E, Becker CM, Lutjen-Drecol E. Dependency of intraocular pressure elevation and glaucomatous changes in DBA/2J and DBA/2J-Rj mice. Invest Ophthalmol Vis Sci 2008;49:613–621. [PubMed: 18235006]

Schori H, Kipnis J, Yoles E, WoldeMussie E, Ruiz G, Wheeler LA, Schwartz M. Vaccination for protection of retinal ganglion cells against death from glutamate cytotoxicity and ocular hypertension: implications for glaucoma. Proc Natl Acad Sci USA 2001;98:3398–3403. [PubMed: 11248090]

Shareef SR, Garcia-Valenzuela E, Salierno A, Walsh J, Sharma SC. Chronic ocular hypertension following episcleral venous occlusion in rats. Exp Eye Res 1995;61:379–382. [PubMed: 7556500]

Soto I, Oglesby E, Buckingham BP, Son JL, Roberson ED, Steele MR, Inman DM, Vetter ML, Horner PJ, Marsh-Armstrong N. Retinal ganglion cells downregulate gene expression and lose their axons within the optic nerve head in a mouse glaucoma model. J Neurosci 2008;28:548–561. [PubMed: 18184797]

Ueda J, Sawaguchi S, Hanyu T, Yaoeda K, Fakushi T, Abe H, Ozawa H. Experimental glaucoma model in the rat induced by laser trabecular photocoagulation after an intracameral injection of India ink. Jpn J Ophthalmol 1998;42:337–344. [PubMed: 9822959]

Urcola JH, Hernandez M, Vecino E. Three experimental glaucoma models in rats: Comparison of the effects of intraocular pressure elevation on retina ganglion cell size and death. Exp Eye Res 2006;83:429–437. [PubMed: 16682027]

Weber AJ, Zelenak D. Experimental glaucoma in the primate induced by latex microspheres. J Neurosci Methods 2001;111:39–48. [PubMed: 11574118]

Yang Z, Quigley HA, Pease ME, Yang Y, Qian J, Valenta D, Zack DJ. Changes in gene expression in experimental glaucoma and optic nerve transection: The equilibrium between protective and detrimental mechanisms. Invest Ophthalmol Vis Sci 2007;48:5539–5548. [PubMed: 18055803]

Zhou Y, Grinchuk O, Tomarev SI. Transgenic mice expressing the Tyr437His mutant of human myocilin protein develop glaucoma. Invest Ophthalmol Vis Sci 2008;49:1932–1939. [PubMed: 18436825]

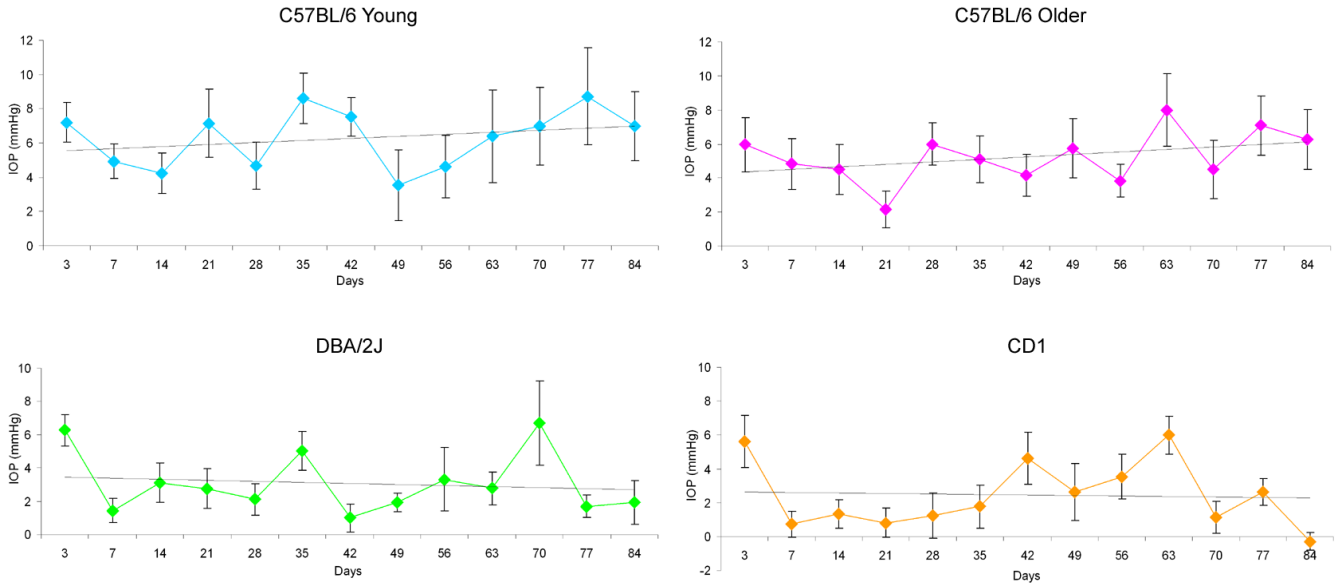

Figure 1.

Difference between bead-injected eyes and fellow control eyes expressed as mean ± standard error IOP (mmHg) for C57BL/6 younger, C57BL/6 older, DBA/2J younger, and CD1 younger mice throughout study. Linear regression of mean values for each time point included in each of 4 graphs.

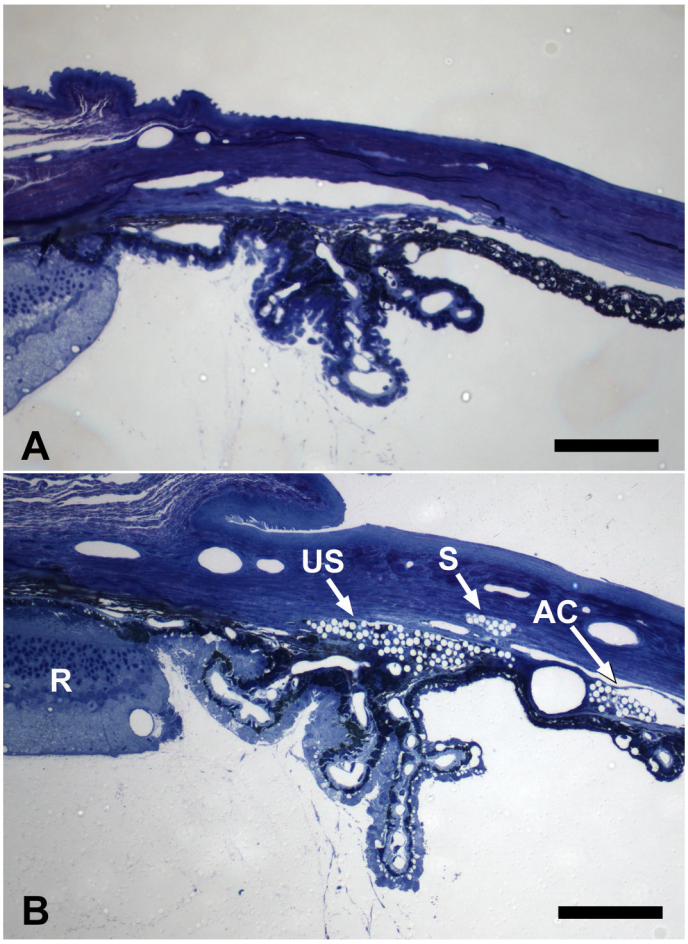

Figure 2.

A: Anterior segment of control, non-injected, C57BL/6 younger mouse. B: Anterior segment of C57BL/6 younger mouse 6 weeks after bead injection. Beads are seen as clear spheres due to extraction of polystyrene during epoxy embedding. Beads are found in the iris stroma, in the uveoscleral pathway between ciliary body and sclera (US) and in outflow channels equivalent to Schlemm's canal (S). Anterior chamber (AC), Retina (R). (1% toluidine blue; scale bars = 70μm)."

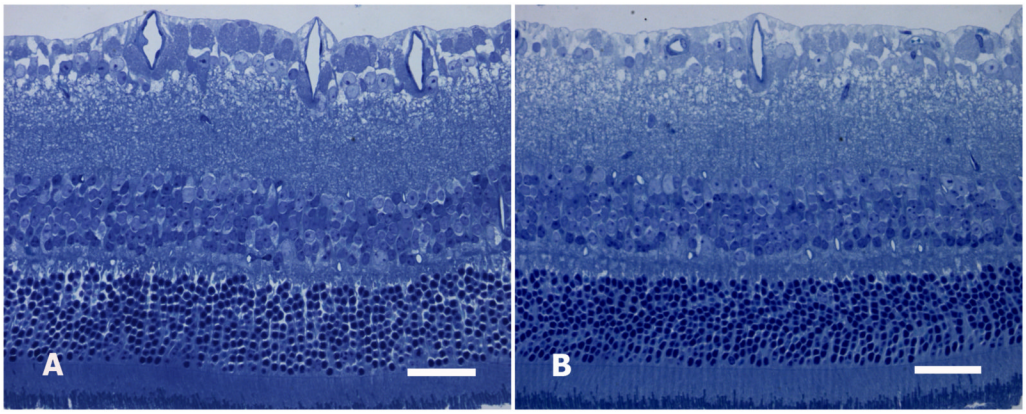

Figure 3.
CD1 mouse retinas 12 weeks after bead injection. A: Normal mouse retina. B: Bead-injected mouse retina showing thinning of nerve fiber and RGC layer, but normal thickness of inner nuclear and outer nuclear layers (1% toluidine blue stain; scale bar = 30μm).

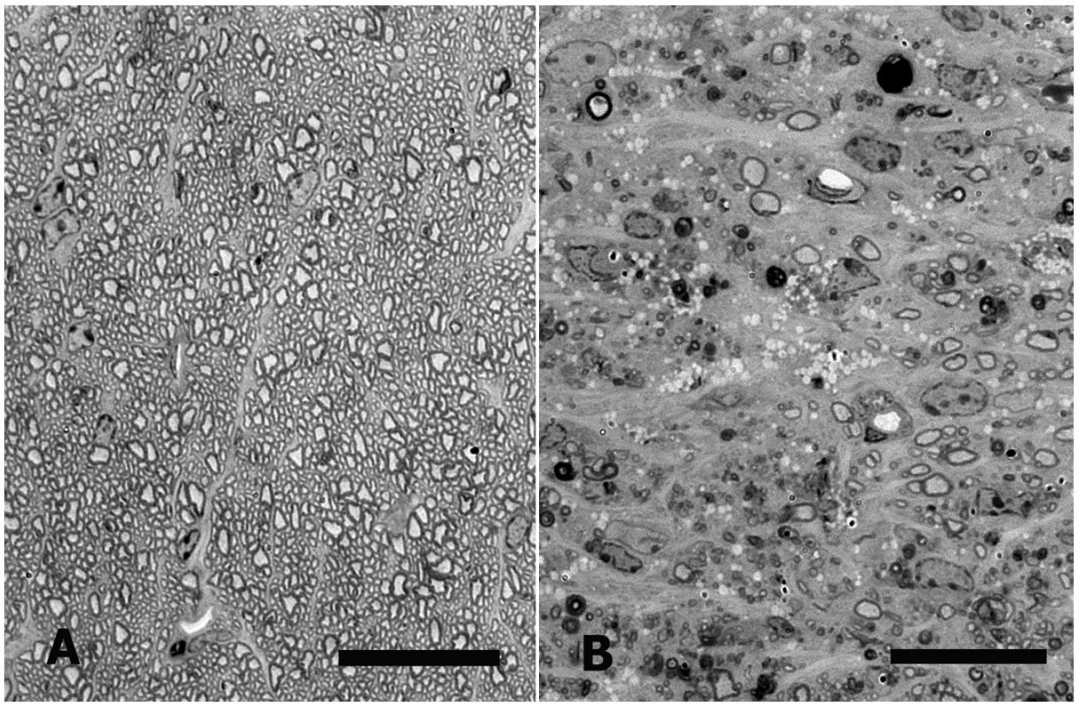

Figure 4.
Optic nerve cross-sections from CD1 mice. A: Normal mouse optic nerve. B: Nerve from bead-injected eye 12 weeks after injection, showing major loss of normal axon profiles, as well as clumps of myelin debris and macrophages filled with clear vacuoles (epoxy-embedded, 1 μm section, 1% toluidine blue, scale bars = 20 μm).

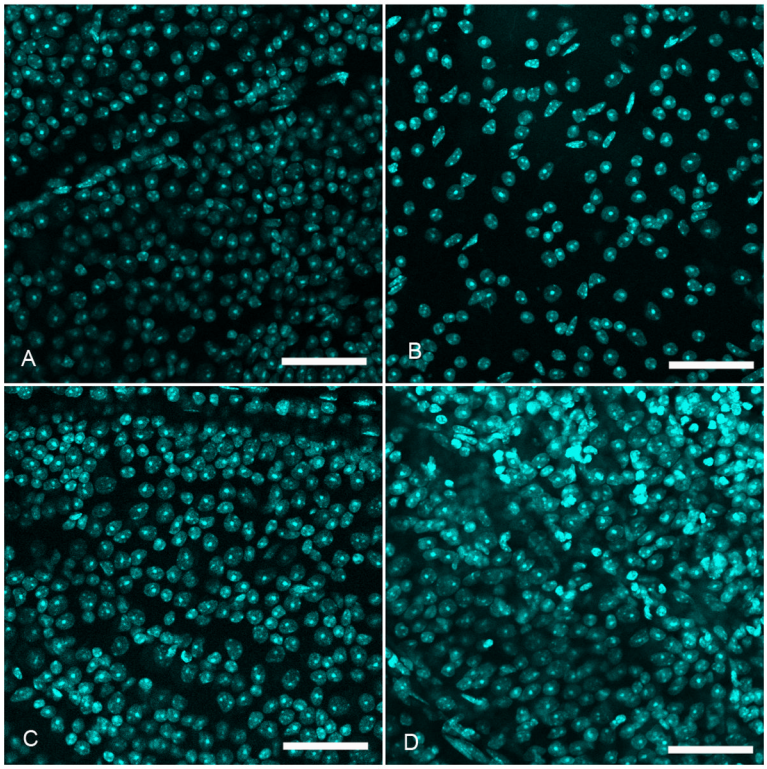

Figure 5.
Retinal whole mounts in confocal micrographs of CD1 mice 12 weeks after bead injection. A and C: control retinas. B: shows significant cell loss in the RGC layer after bead injection. D: one of the rare examples of a excluded retinal whole mount showing increased RGC layer cells due to an inflammatory infiltrate (superior retina, DAPI stain, scale bars = 50 μm).

Table 1

IOP Data

			MEAN ± SD	MEAN ± SD	MEAN ± SD	Median IOP	Positive	Average #	Percent IOP
Strain	**n**	**Duration**	**RE IOP (mmHg)**	**LE IOP (mmHg)**	**IOP diff (mmHg)**	**diff LE-RE (mmHg)**	**Integral**	**IOP elevations**	**elevations**
C57/BL6 younger	9	3 weeks	11.2 ± 1.1	26.3 ± 7.6	15.1 ± 7.6	18	231 ± 144.7	2.4 ± 0.9	70% ± 26%
C57/BL6 younger	27	6 weeks	9.8 ± 1.1	15.3 ± 4.6	5.5 ± 4.2	5	196 ± 158.7	3.3 ± 2.0	47% ± 29%
C57/BL6 younger	13	12 weeks	9.8 ± 1.0	14.4 ± 4.0	4.7 ± 3.8	5	397 ± 260.4	5.5 ± 2.4	40%± 21%
C57/BL6 older	12	6 weeks	9.8 ± 1.3	14.5 ± 4.0	4.8 ± 4.5	4	179 ± 152.9	2.8 ± 2.3	39% ± 32%
C57/BL6 older	12	12 weeks	11.2 ± 0.8	16.4 ± 2.5	5.3 ± 2.6	5	421 ± 234.8	6.8 ± 3.1	61% ± 24%
DBA/2J younger	12	6 weeks	11.1 ± 1.0	14.9 ± 1.5	3.8 ± 1.3	3	142 ± 76.0	2.9 ± 1.3	42% ± 19%
DBA/2J younger	13	12 weeks	10.7 ± 0.9	13.0 ± 2.6	3.1 ± 3.1	2	226 ± 254.2	3.1 ± 3.1	24% ± 24%
CD1 younger	10	6 weeks	10.3 ± 0.8	11.8 ± 2.0	1.5 ± 2.5	1.5	68 ± 55.4	1.5 ± 1.0	21% ± 14%
CD1 younger	11	12 weeks	10.3 ± 0.8	13.5 ± 3.2	3.2 ± 3.5	2	255 ± 265.5	4.4 ± 3.2	34% ± 25%
Total	119								42%

Mean and median intraocular pressures (IOP, in mmHg) for right eye (RE) and left eye (LE), diff = difference LE-RE, positive integral IOP (see explanation in Methods), number of IOP elevations throughout study duration, and IOP percent elevations of all measurements. Elevation defined as exceeding the 97.5% confidence interval for interocular IOP difference in normal mice (5 mmHg). Values are given as mean ± standard deviation, except for median IOP difference LE-RE. Sample number (N)

Table 2

Axial length and width changes with induced IOP elevation.

			Control eyes		Bead eyes		Increase	Increase	% length
Strain	**Weeks**	**N**	**Length**	**Width**	**Length**	**Width**	**Length**	**Width**	**change (P)**
C57/BL6 younger	6	27	3.32 ± 0.15	3.21 ± 0.15	3.77 ± 0.33	3.47 ± 0.49	13.6%	8.1%	**<0.0001**
C57/BL6 older	6	12	3.43 ± 0.10	3.23 ± 0.13	3.60 ± 0.22	3.47 ± 0.19	5.2%	6.7%	**0.02**
C57/BL6 older	12	12	3.68 ± 0.10	3.44 ± 0.12	3.99 ± 0.35	3.68 ± 0.22	8.3%	6.9%	**0.007**
CD1	6	10	3.56 ± 0.11	3.32 ± 0.09	3.80± 0.20	3.51 ± 0.13	6.8%	5.9%	**<0.0001**
CD1	12	11	3.58 ± 0.09	3.47 ± 0.12	3.73 ± 0.25	3.63 ± 0.25	4.3%	4.6%	0.08
DBA/2J younger	6	12	3.35 ± 0.08	3.25 ± 0.12	4.19 ± 0.26	3.65 ± 0.21	25.3%	12.4%	**<0.0001**
DBA/2J younger	12	13	3.50 ± 0.10	3.29 ± 0.11	3.80 ± 0.18	3.59 ± 0.16	8.7%	8.3%	**<0.0001**
DBA/2J older	50	55			3.83 ± 0.23	3.69 ± 0.27	14.3%	13.5%	**<0.0001**

Length and width values are mean ± standard deviation; included here are axial length measurements from spontaneous glaucoma, DBA/2J older mice (mean age 55 weeks) compared to younger DBA/2J uninjected eyes; p values from t tests. Sample number (N)

Table 3

Axial length percent increase in experimental compared to control eyes.

			p* diff		p†, unadjusted difference			p‡, adjusted for IOP exposure		
Strains	**N**	**mean ± sd**	**bead--control**	**median**	**C57 young**	**C57 old**	**CD1**	**C57 young**	**C57 old**	**CD1**
DBA/2J	25	16.7 ± 10.7%	**<0.0001**	15.8%	0.14	**0.0007**	**0.0003**	0.38	**0.0026**	**0.0003**
C57BL/6 younger	20	13.6 ± 14.1%	**0.0004**	12.4%		**0.02**	**0.01**		0.07	0.08
C57BL/6 older	24	6.8 ± 7.7 %	**0.0003**	4.9%			0.94			0.33
CD1	21	5.5 ± 6.7 %	**0.001**	5.7%						

Sample number (N) and standard deviation (SD).

*paired t test;

†Mann-Whitney test; from multivariable linear regression,

‡adjusting for positive integral IOP; for each strain values for 6 and 12 week duration are grouped together.

Table 4

Mean RGC layer loss and axon loss (bead injected compared to control) for each strain at 6 or 12 weeks.

	Axon loss, 6 weeks			Axon loss, 12 weeks			RGC layer loss, 6 weeks			RGC layer loss, 12 weeks		
Strain	**N**	**mean ± SD**	**median**	**N**	**mean ± SD**	**median**	**N**	**mean ± SD**	**median**	**N**	**mean ± SD**	**median**
CD1	10	12.9 ± 11.8%†	12.0%	10	32.0 ± 28.3%†	25.2%	10	9.9 ± 9.5%†	10.4%	10	20.1 ± 15.7% †	15.1%
C57BL/6 younger	14	15.9 ± 23.5%†	9.3%	10	6.5 ± 8.9%*	6.5%	14	9.3 ± 6.5%†	9.0%	10	5.2 ± 12.1%	6.9%
DBA/2J	11	7.1 ± 7.6%†	7.3%	13	13.9 ± 27.8%	4.8%	12	9.1 ± 7.4%†	9.1%	12	4.1 ± 16.5%	1.6%
C57BL/6 older	12	10.5 ± 19.6%	5.4%	12	0.1 ± 8.2%	−0.3%	12	0.0 ± 6.7%	−0.3%	12	4.1 ± 7.3%	2.4%

Sample number (N), standard deviation (SD).

*$p < 0.05$,

†$p < 0.01$ for difference between injected and fellow eye, t test.

Table 5

Axon counts.

		Axon	Axon	Axon Loss	p* diff	Axon Loss	p†, unadjusted difference from			p‡, adjusted for IOP exposure		
Strain	**N**	**RE Mean Count**	**LE Mean Count**	**mean loss ± SD**	**bead--control**	**median loss**	**C57 young**	**DBA/2J**	**C57 old**	**C57 young**	**DBA/2J**	**C57 old**
CD1	20	60995 ± 6994	48708 ± 15496	22.5 ± 23.3%	**0.0004**	16.00%	0.07	**0.023**	**0.003**	0.16	0.098	**0.017**
C57/BL6 younger	24	51064 ± 5045	43045 ± 12802	11.9 ± 19.1%	**0.007**	6.90%		0.73	0.09		0.83	0.26
DBA/2J	24	60938 ± 5553	54380 ± 13097	10.8 ± 21.0%	**0.02**	6.20%			0.26			0.43
C57/BL6 older	24	47113 ± 6510	44618 ± 7164	5.2 ± 15.6%	0.22	1.20%						

Bead injected (LE) RGC mean and median loss counts were compared to the average values of fellow right eyes (RE) of the same strain followed for the same time period (6 or 12 weeks). Sample number (N), standard deviation (SD), and difference (diff).

*paired t test;

†Mann-Whitney test; from multivariable linear regression,

‡adjusting for positive integral IOP;

Table 6

RGC layer counts.

		RGC Layer Control	RGC Layer Bead Injected	RGC layer	p* diff	RGC layer	p†, unadjusted difference from			p‡, adjusted for IOP exposure		
Strain	**N**	**Mean Count**	**Mean Count**	**mean loss ± SD**	**bead-control**	**median loss**	**C57 young**	**DBA/2J**	**C57 old**	**C57 young**	**DBA/2J**	**C57 old**
CD1	20	3820 ± 232	3247 ± 518	15.0 ± 13.7%	**<0.0001**	12.70%	**0.044**	**0.02**	**0.0003**	**0.029**	**0.03**	**<0.0001**
C57/BL6 younger	23	4196 ± 406	3851 ± 423	7.5 ± 9.4%	**0.007**	7.40%		0.31	**0.011**		0.78	**0.024**
DBA/2J	24	4121 ± 262	3849 ± 512	6.6 ± 12.8%	**0.04**	3.80%			0.19			0.081
C57/BL6 older	24	3921 ± 236	3798 ± 260	2.0 ± 7.1%	0.1	1.20%						

RGC layer counts comparing mean and median loss in bead-injected (left eye) to the average values of fellow, right eyes of the same strain followed for the same time period (6 or 12 weeks), as well as comparisons of loss among strains of mice. Sample number (N), standard deviation (SD).

*paired t test;

†Mann-Whitney test; from multivariable regression,

‡adjusting for positive integral IOP.